Supplementary Information for Chang, W. et. al., "Probabilistic calibration of a Greenland Ice Sheet model using spatially-resolved synthetic observations: toward projections of ice mass loss with uncertainties"

1. Gaussian process emulator for principal components

In this section, we outline our statistical approach for ice sheet model emulation using Gaussian process (GP) models and principal component (PC) analysis (often referred to as empirical orthogonal functions, EOFs). Our approach follows Chang et al. (2013) in that we summarize the ice sheet model runs as PCs and calibrate the ice sheet parameters based on GP emulators for PCs. Our description of methods below therefore also closely follows the notation and description in Chang et al. (2013). By decomposing spatial patterns into a small number of variables representing important characteristics of model runs, our approach drastically increases computational efficiency without causing significant information loss.

We denote the number of model runs by p and the number of spatial locations spatial locations by n. For the SICOPOLIS model output (from Applegate et al. 2012) we use here, $p = 99$ and $n = 264$. We let $Y(\boldsymbol{\theta}, \mathbf{s})$ denote the ice thickness from the ice sheet model at a parameter setting $\boldsymbol{\theta} = (\theta_1, \ldots, \theta_5)^T$ and a spatial location $\mathbf{s}$. We let $\mathbf{s}_1, \ldots, \mathbf{s}_n$ be the spatial locations of the model grid points and $\mathbf{Y}(\boldsymbol{\theta}) = (Y(\boldsymbol{\theta}, \mathbf{s}_1), \ldots, Y(\boldsymbol{\theta}, \mathbf{s}_n))$ be the vector

of model output at a parameter setting $\boldsymbol{\theta}$. Let $\boldsymbol{\theta}_1, \ldots, \boldsymbol{\theta}_p$ be the vectors of input parameters for our model. $\mathbf{Y}$ is an $n \times p$ matrix of the ice sheet model output where its rows correspond to spatial locations and columns to parameter settings, i.e.

$$\mathbf{Y} = \begin{pmatrix} Y(\boldsymbol{\theta}_1, \mathbf{s}_1), & Y(\boldsymbol{\theta}_2, \mathbf{s}_1), & \ldots, & Y(\boldsymbol{\theta}_p, \mathbf{s}_1) \\ Y(\boldsymbol{\theta}_1, \mathbf{s}_2), & Y(\boldsymbol{\theta}_2, \mathbf{s}_2), & \ldots, & Y(\boldsymbol{\theta}_p, \mathbf{s}_2) \\ \vdots, & \vdots, & \ddots, & \vdots \\ Y(\boldsymbol{\theta}_1, \mathbf{s}_n), & Y(\boldsymbol{\theta}_2, \mathbf{s}_p), & \ldots, & Y(\boldsymbol{\theta}_p, \mathbf{s}_n) \end{pmatrix}.$$

Similarly, $Z(\mathbf{s})$ denotes the observed ice sheet thickness at a location $\mathbf{s}$, and $\mathbf{Z} = (Z(\mathbf{s}_1), \ldots, Z(\mathbf{s}_n))^T$ is the $n \times 1$ vector of the observational data.

2. Principal component analysis for model output

The first step is summarizing the model output by principal component analysis. Following the standard procedure of principal component analysis, the column means are subtracted from each element in the corresponding columns such that each column is centered on zero. We apply singular value decomposition to this centered output matrix to find the scaled principal basis vectors $\mathbf{k}_1 = \sqrt{\lambda_1}\mathbf{e}_1, \ldots, \mathbf{k}_p = \sqrt{\lambda_p}\mathbf{e}_p$, where $\lambda_1 > \lambda_2 > \cdots > \lambda_p$ and $\mathbf{e}_1, \ldots, \mathbf{e}_p$ are ordered eigenvalues and their eigenvectors respectively. Each eigenvalue represents the explained variation for the corresponding principal component. We keep only the first $J \ll p$ PCs with the largest explained variation (i.e. the largest eigenvalues) to minimize the information loss due to dimension reduction. The principal components for model output can be computed by

$$\mathbf{Y}^R = (\mathbf{K}_y^T \mathbf{K}_y)^{-1} \mathbf{K}_y^T \mathbf{Y} = (\mathbf{Y}_1^R \ldots \mathbf{Y}_J^R)^T$$

where $\mathbf{K}_y = (\mathbf{k}_1, \ldots, \mathbf{k}_J)$ is the principal basis matrix. $\mathbf{Y}_i^R = (Y_i^R(\boldsymbol{\theta}_1), \ldots, Y_i^R(\boldsymbol{\theta}_p))^T$ is the $p \times 1$ vector of the ith principal components, and $Y_i^R(\boldsymbol{\theta}_j)$ is the ith principal component at the parameter setting $\boldsymbol{\theta}_j$. The resulting matrix $\mathbf{Y}^R$ is the summarized output matrix with

rows for PCs and columns for parameter settings . The procedure reduces the size of the data from $n \times p$ to $J \times p$.

3. Gaussian process emulator

We emulate the ice sheet model output using Gaussian processes (GP), a fast method for probabilistic interpolation between existing model runs (Sacks et al. 1989; Higdon et al. 2008; Drignei et al. 2008; Holden et al. 2010; Bhat et al. 2012; Olson et al. 2012, 2013) . The GP emulator approach yields a flexible approximation without requiring detailed physical information on the ice sheet model, unlike linear regression-based emulators (cf. Piani et al. 2005). Moreover, in addition to its optimality in interpolating smoothly varying functions, the method enables a natural quantification of uncertainty. The interpolator is essentially a random process with a mean that the optimal interpolation between ice sheet model runs in terms of the expected mean squared error and a variance that quantifies the uncertainty of the interpolation.

Because the principal components are uncorrelated with each other by construction, we can model each of them separately using independent GPs. Note that this basically ignores the dependence between the principal components that is not captured by the covariances. However, according to our experiences for various models including SICOPOLIS, the emulator based on this assumption usually provides a very accurate approximation to the original model that is being emulated. We model each $\mathbf{Y}_i^R$ using a GP with mean zero and covariance determined by the following squared exponential covariance function:

$$Cov(Y_i^R(\boldsymbol{\theta}_j), Y_i^R(\boldsymbol{\theta}_k); \zeta_i, \kappa_{y,i}, \phi_i) = \zeta_i 1(\boldsymbol{\theta}_j = \boldsymbol{\theta}_k) + \kappa_{y,i} \exp\left(- \sum_{l=1}^{5} \left(\frac{\theta_{jl} - \theta_{kl}}{\phi_{il}} \right)^2 \right),$$

where $\zeta_i, \kappa_{y,i}, \phi_{i1}, \ldots, \phi_{i5} > 0$ are covariance parameters, θ_{jl} is the lth element of $\boldsymbol{\theta}_j$, and $1(\cdot)$ is the index function. The covariance parameters $(\zeta_1, \kappa_{1,y}, \phi_{11}, \ldots, \phi_{15}), \ldots, (\zeta_J, \kappa_{y,J}, \phi_{J1}, \ldots, \phi_{J5})$ are estimated by maximum likelihood estimation (MLE). Our emulator, denoted by $J \times 1$ vector-valued function $\boldsymbol{\eta}(\boldsymbol{\theta}, \mathbf{Y}^R)$, is the predictive distribution of PCs at an untried param-

eter setting $\boldsymbol{\theta}$ defined by the fitted GPs. Using the PC emulator, we can also emulate the original model transect by computing $\mathbf{K}_y\boldsymbol{\eta}(\boldsymbol{\theta}, \mathbf{Y}^R)$.

Note that our approach allows significant improvements in computational efficiency. Without any dimension reduction, the computational cost for a single likelihood evaluation scales as $\mathcal{O}(n^3p^3)$, which corresponds to a few hours of computing time. Thus, application of any numerical methods requiring repeated evaluation of the likelihood function is computationally prohibitive if no dimensional reduction is performed. Our approach decreases the computational complexity to $\mathcal{O}(Jp^3)$, and this is a reduction from 3.18×10^{14} flops to 1.56×10^8 flops in our case. The computing time reduces to less than a second for a single likelihood evaluation.

4. Model parameter calibration

In this section, we formulate the probability model for calibration using the PC emulator constructed above and explain the inference procedure for the model parameters using Markov chain Monte Carlo (MCMC).

We assume that the observational dataset is emulator output contaminated by model discrepancy and observational error;

$$\mathbf{Z} = \mathbf{K}_y\boldsymbol{\eta}(\boldsymbol{\theta}^*, \mathbf{Y}^R) + \mathbf{K}_d\boldsymbol{\nu} + \boldsymbol{\epsilon}, \tag{S1}$$

where $\boldsymbol{\theta}^*$ is the best fit input parameter setting (Bayarri et al. 2007) for the observational data, and $\boldsymbol{\epsilon} \sim N(0, \sigma^2\mathbf{I}_n)$ is the observational error with variance $\sigma^2 > 0$. $\mathbf{K}_d\boldsymbol{\nu}$ is the model-observation discrepancy picking up systematic differences between the model and the observations (cf. Bayarri et al. 2007; Bhat et al. 2012), where $\mathbf{K}_d$ is a kernel basis matrix relating the spatial locations $\mathbf{s}_1, \ldots, \mathbf{s}_n$ to J_d knot locations $\mathbf{a}_1, \ldots, \mathbf{a}_{J_d}$, and $\boldsymbol{\nu} \sim N(\mathbf{0}, \kappa_d\mathbf{I}_{J_d})$ is the vector of knot processes, a set of random variables assigned to each of the knot locations with variance $\kappa_d > 0$. Our choice for the kernel function is an exponential covariance given

by

$$\{\mathbf{K}_d\}_{ij} = \exp\left(-\frac{|\mathbf{s}_i - \mathbf{a}_j|}{\phi_d}\right),$$

with $\phi_d > 0$. The variance parameter κ_d is subject to inference, and the correlation parameter ϕ_d is pre-specified by expert judgment. In our implementation, we choose ϕ_d as 5% of the maximum distance between the spatial locations on the model grid to yields a sufficiently flexible discrepancy pattern. Note that the kernel basis often needs to be substituted by its scaled principal basis (eigenvectors) to improve identifiability. See Chang et al. (2013) for a more detailed discussion. We used the 30 leading principal basis for $\mathbf{K}_d$ in our implementation. We apply a similar dimension reduction described in the previous section to find $\mathbf{Z}^R$, a summary of the observed transect as follows:

$$\mathbf{Z}^R = (\mathbf{K}^T\mathbf{K})^{-1}\mathbf{K}^T\mathbf{Z}, \tag{S2}$$

and therefore the model for $\mathbf{Z}^R$ can be written as

$$\mathbf{Z}^R \sim N\left(\begin{pmatrix} \boldsymbol{\mu}_{\boldsymbol{\eta}} \\ \mathbf{0} \end{pmatrix}, \begin{pmatrix} \Sigma_{\boldsymbol{\eta}} & \mathbf{0} \\ \mathbf{0} & \kappa_d \mathbf{I}_{J_d} \end{pmatrix} + \sigma^2(\mathbf{K}^T\mathbf{K})^{-1}\right),$$

where $\mu_{\boldsymbol{\eta}}$ and $\Sigma_{\boldsymbol{\eta}}$ are the mean and covariance, respectively, of the emulator $\boldsymbol{\eta}(\boldsymbol{\theta}^*, \mathbf{Y}^R)$.

The parameters to be estimated in the calibration model are the ice sheet model input parameters $\boldsymbol{\theta}^*$, the discrepancy parameter κ_d, and the observational error variance σ^2. We also re-estimate the partial sill parameters $\boldsymbol{\kappa}_y = (\kappa_{y,1}, \ldots, \kappa_{y,J})$ for the emulator (Bayarri et al. 2007; Bhat et al. 2012; Chang et al. 2013). We define the posterior density based on the likelihood function given by (S2) denoted by $\ell(\mathbf{Z}^R|\boldsymbol{\theta}^*, \boldsymbol{\kappa}_y, \kappa_d, \sigma^2, \mathbf{Y}^R)$ and some standard prior specifications denoted by $f(\boldsymbol{\theta}^*)$, $f(\boldsymbol{\kappa}_y)$, $f(\kappa_d)$, and $f(\sigma^2)$ (Higdon et al. 2008; Chang et al. 2013). Each of the input parameters in $\boldsymbol{\theta}^*$ receives a flat prior on a broad range determined by model ensemble design and physical knowledge. The observational error variance σ^2 and the variance for the discrepancy κ_d have non-informative inverse-gamma priors with small shape parameters. We specify somewhat informative priors for $\kappa_{y,1}, \ldots, \kappa_{y,J}$ by specifying a large shape parameter in order to avoid numerical instability and identifiability issues

(Higdon et al. 2008). The posterior distribution resulting from the above model is

$$\pi(\boldsymbol{\theta}^*, \boldsymbol{\kappa}_y, \kappa_d, \sigma^2 | \mathbf{Z}^R, \mathbf{Y}^R) \propto \ell(\mathbf{Z}^R | \boldsymbol{\theta}^*, \boldsymbol{\kappa}_y, \kappa_d, \sigma^2, \mathbf{Y}^R) f(\boldsymbol{\theta}^*) f(\boldsymbol{\kappa}_y) f(\kappa_d) f(\sigma^2),$$

where

$$\begin{aligned}
\ell(\mathbf{Z}^R | \boldsymbol{\theta}^*, \boldsymbol{\kappa}_y, \kappa_d, \sigma^2, \mathbf{Y}^R) &\propto \left|\Sigma_{\boldsymbol{\eta}} + \mathbf{K}^T \mathbf{K} \sigma^2\right|^{-\frac{1}{2}} \exp\left(-\frac{1}{2} \mathbf{Z}^{R^T} \left(\Sigma_{\boldsymbol{\eta}} + \mathbf{K}^T \mathbf{K} \sigma^2\right)^{-1} \mathbf{Z}^R\right) \\
f(\boldsymbol{\theta}^*) &\propto 1(\boldsymbol{\theta}^* \in \Theta),\ \Theta \text{ represents the range of } \boldsymbol{\theta}, \\
f(\boldsymbol{\kappa}_y) &\propto \prod_{i=1}^{J} \kappa_{y,i}^{-a_{y,i}-1} \exp\left(-\frac{b_{y,i}}{\kappa_{y,i}}\right),\ a_{y,1}, \ldots, a_{y,J}, b_{y,1}, \ldots, b_{y,J} > 0 \\
f(\kappa_d) &\propto \kappa_d^{-a_d-1} \exp\left(-\frac{b_d}{\kappa_d}\right),\ a_d, b_d > 0 \\
f(\sigma^2) &\propto \sigma^{-2(a_\sigma+1)} \exp\left(-\frac{b_\sigma}{\sigma^2}\right),\ a_\sigma, b_\sigma > 0.
\end{aligned}$$

For each i, we set $a_{y,i} = 50$ and choose $b_{y,i}$ such that the mode of the prior density $b_{y,i}/(a_{y,i}+1)$ coincides with the MLE of $\kappa_{y,i}$ computed in the emulation stage. For other parameters, we impose vague priors by setting $a_d = 2$, $b_d = 3$, $a_\sigma = 2$, and $b_\sigma = 3$.

The synthetic observations used in our perfect model experiment are constructed by superimposing a random error generated from a Gaussian process model on the assumed true ice sheet status (run # 67). The covariance function that we use for the Gaussian process model here is a squared exponential covariance having range of 2100 km, partial sill of 2500 m, and a nugget of 1 m. Our choice for the discrepancy process is based on the following two general assumptions: (i) the discrepancy is statistically identifiable from the emulator process, and (ii) SICOPOLIS has an enough skill to reproduce the observed ice profile. (i) is related to the value of the range parameter, which controls the effective distance at which two spatial locations are uncorrelated. To ensure that the discrepancy process is identifiable from the emulator process, we set the range parameter to be very large (80% of the spatial range of the model output) so that the discrepancy operates in a different spatial scale to the emulator process. (ii) is related to the value of the partial sill, which defines the magnitude of the discrepancy. Here we let the value of the partial sill to be reasonably small to simulate the situation that the structural error is not large

and therefore SICOPOLIS can reproduce the observed ice profile reasonably well. Note that calibration based on any framework including our approach can become problematic if any of the assumptions are violated; if the discrepancy process operates in a similar spatial scale to the emulator process (i.e. (i) does not hold), the discrepancy causes identifiability issues and hence introduces a significant bias in the calibration result. If the magnitude of the discrepancy is too large (i.e. (ii) does not hold) compared to the variation between model outputs, the calibration results will become essentially non-informative (i.e. resulting in a very dispersed posterior density). Note that these are common issues for most existing calibration methods in general.

Based on the pseudo observations, we infer the parameters using the MCMC sample from the above posterior distribution obtained by the Metropolis-Hastings algorithm (cf. Higdon et al. 2009). In particular, we infer the input parameters in $\boldsymbol{\theta}^*$ by investigating their marginal density $\pi(\boldsymbol{\theta}^*|\mathbf{Z}^R, \mathbf{Y}^R)$. In our perfect model experiment, we obtained 300,000 draws using block updating when estimating the full joint density of all five parameters. The computing time takes about eight hours on a single high-performance core. For inference on individual input parameter, only 30,000 draws using block updating is sufficient. In both cases, we confirmed that the Monte Carlo chain is well-mixed by comparing the densities of the first half of the chain with the entire chain. We find the probability density of the input parameters via kernel density estimation for the MCMC sample. The estimated density can be easily plotted for visual analysis as shown in Figures 3 and 4. Note that ignoring the spatially correlated discrepancy results in a notably biased calibration results in our perfect model experiment. See Figure S2 for a comparison of posterior densities with and without the discrepancy term.

5. Ice volume change projection based on calibrated parameters

One important purpose of parameter calibration is making better projections for the future ice sheet mass loss. Making future projections based on calibration results requires a function that relates input parameter values $\boldsymbol{\theta}^*$ to future changes in ice sheet volume. In our illustrative example, the variable that we want to project is the ice volume change from present to 2100 in meters of sea level equivalence. For each model run, we compute the ice volume change by subtracting the current ice volume from the future ice volume. We then obtain a 5-dimensional surface of ice volume change by interpolation between those computed changes.

Among many possible choices for the interpolator, we use the Gaussian process emulator similar to the model described in 3. More specifically, we fit a Gaussian process model for the ice volume change over the input parameter space with zero-mean and the covariance function

$$Cov(\Delta v(\boldsymbol{\theta}_j), \Delta v(\boldsymbol{\theta}_k); \zeta^{vol}, \kappa^{vol}, \phi^{vol}) = \zeta^{vol} 1(\boldsymbol{\theta}_j = \boldsymbol{\theta}_k) + \kappa^{vol} \exp\left(- \sum_{l=1}^{5} \frac{|\theta_{jl} - \theta_{kl}|}{\phi_l^{vol}} \right),$$

for any given design points $\boldsymbol{\theta}_j$ and $\boldsymbol{\theta}_k$ $(j, k = 1, \cdots, 100)$, where $\Delta v(\boldsymbol{\theta})$ is the volume change at a parameter setting $\boldsymbol{\theta}$, and $\zeta^{vol}.\kappa^{vol}, \phi_1^{vol}, \ldots, \phi_5^{vol} > 0$ are the covariance parameters that need to be estimated via MLE. The resulting function can predict ice volume change at any given value of $\boldsymbol{\theta}$ as the conditional mean given by the standard kriging approach (Cressie 1993). Figure S1 shows the marginal surface of the projection as a function of input parameters. To validate the emulator constructed here, we have conducted leave-5-percent-out cross validation and the mean error rate is around 16%; the error rate is a little higher than the heuristic upper limit for the generally acceptable emulation error (10%) due to the irregular behavior of the volume change surface.

We obtain a Monte Carlo sample of ice volume projections by supplying the posterior sample of the calibrated parameters to the interpolation function. Each element of the posterior sample is converted to ice volume change. The predictive density of the ice volume projection can be found by applying kernel density estimation. We find the prior density of the projections in the same manner; we convert the design points of the existing model runs

into the ice volume changes and compute the predictive density for it using kernel density estimation.

To investigate whether the perfect model experiment results shown in the main text are sensitive to the values of input parameters assumed as the synthetic truth, we have conducted perfect model experiments for additional parameter settings other than the one used in the manuscript. As illustrative examples, we below present the calibrated ice volume change projections (Figure S3 and S4) for two input parameter settings that result in the minimum and the maximum projected ice volume changes from 2005 to 2100 among the parameter settings that produce the modern ice volumes within 15 percent of the observed ice volume (Bamber et al. 2001). The results are essentially the same as the one presented in the manuscript; the densities of projected sea level rise peak around the true sea level rise values and the projection uncertainties have been significantly reduced comparing to the simpler method by Applegate et al. (2012).

6. Summary

We describe an ice sheet model calibration approach based on PCs of the model output and the observational data. We build a GP emulator for the PCs of the model output as a fast approximation to the ice sheet model. The calibration model links the observed PCs with the input parameters using the GP emulator while taking the systematic discrepancy into account. We infer the input parameters along with other statistical parameters in the calibration model using MCMC. Combined with projections generated by the ice sheet model, the resulting posterior density of the parameters provide calibrated probabilistic projections of the future ice sheet volume changes.

REFERENCES

Applegate, P., N. Kirchner, E. Stone, K. Keller, and R. Greve, 2012: An assessment of key model parametric uncertainties in projections of Greenland Ice Sheet behavior. *The Cryosphere*, **6 (3)**, 589–606.

Bamber, J., R. Layberry, and S. Gogineni, 2001: A new ice thickness and bed data set for the greenland ice sheet: 1. measurement, data reduction, and errors. **106 (D24)**, 33 773–33 780.

Bayarri, M., et al., 2007: Computer model validation with functional output. **35 (5)**, 1874–1906.

Bhat, K., M. Haran, R. Olson, and K. Keller, 2012: Inferring likelihoods and climate system characteristics from climate models and multiple tracers. *Environmetrics*, **23 (4)**, 345–362.

Chang, W., M. Haran, R. Olson, and K. Keller, 2013: Fast dimension-reduced climate model calibration. *arXiv preprint arXiv:1303.1382, revised and resubmitted the Annals of Applied Statistics*.

Cressie, N., 1993: *Statistics for spatial data*. Wiley, New York.

Drignei, D., C. Forest, and D. Nychka, 2008: Parameter estimation for computationally intensive nonlinear regression with an application to climate modeling. **2 (4)**, 1217–1230.

Higdon, D., J. Gattiker, B. Williams, and M. Rightley, 2008: Computer model calibration using high-dimensional output. **103 (482)**, 570–583.

Higdon, D., C. Reese, J. Moulton, J. Vrugt, and C. Fox, 2009: Posterior exploration for computationally intensive forward models. *Handbook of Markov Chain Monte Carlo*.

Holden, P. B., N. Edwards, K. Oliver, T. Lenton, and R. Wilkinson, 2010: A probabilistic calibration of climate sensitivity and terrestrial carbon change in genie-1. *Climate dynamics*, **35 (5)**, 785–806.

Olson, R., R. Sriver, M. Goes, N. Urban, H. Matthews, M. Haran, and K. Keller, 2012: A climate sensitivity estimate using Bayesian fusion of instrumental observations and an Earth System model. **117 (D4)**, D04 103, doi:10.1029/2011JD016 620.

Olson, R., R. Sriver, M. Haran, W. Chang, N. Urban, and K. Keller, 2013: What is the effect of unresolved internal climate variability on climate sensitivity estimates? **118 (10)**, 4348–4358.

Piani, C., D. Frame, D. Stainforth, and M. Allen, 2005: Constraints on climate change from a multi-thousand member ensemble of simulations. *Geophysical Research Letters*, **32 (23)**.

Sacks, J., W. Welch, T. Mitchell, and H. Wynn, 1989: Design and analysis of computer experiments. **4 (4)**, 409–423.

List of Figures

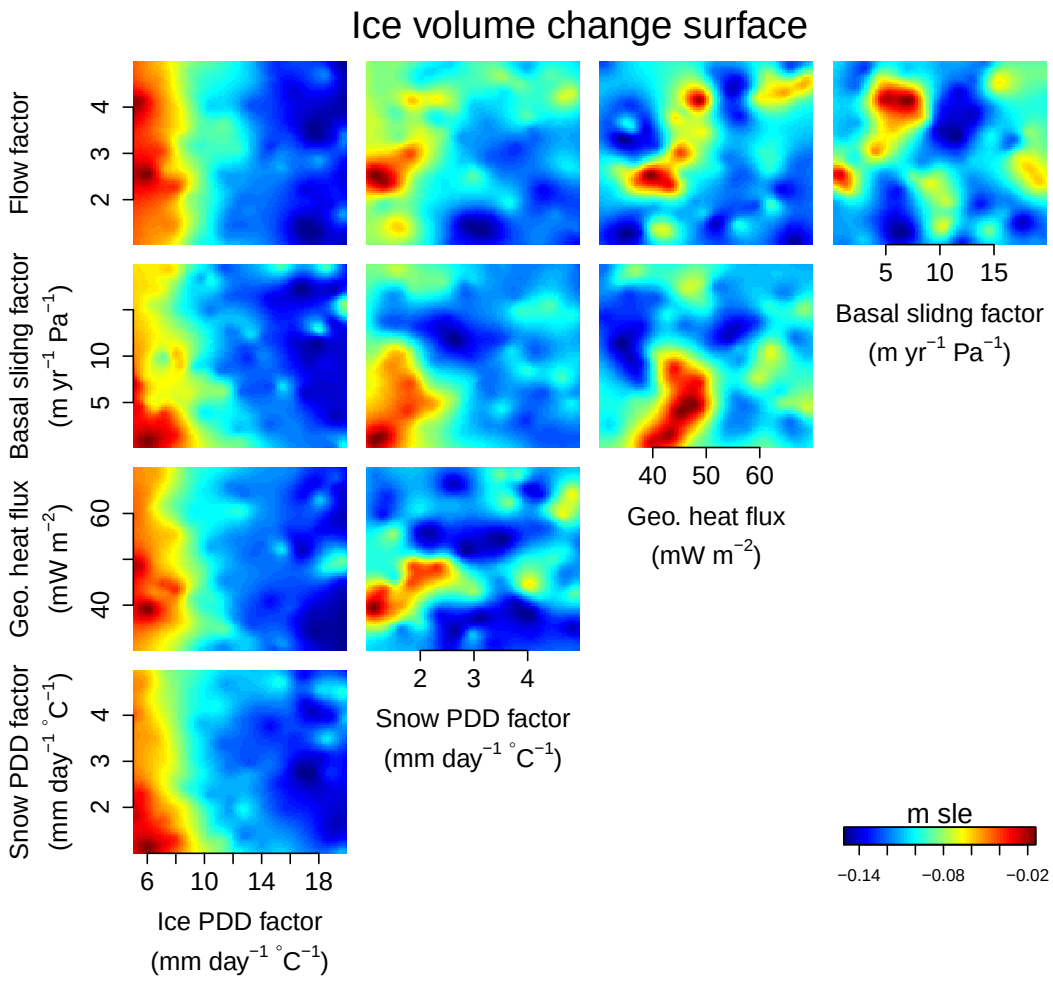

FIG. S1. Surfaces of ice volume change projections between 2005 and 2100 projected onto marginal spaces of all pairs of input parameters. Many local maxima and minima are scattered around the parameter space, indicating that the surfaces behave very irregularly and exhibit highly nonlinear relationship with the input parameters. m sle, meters of sea level equivalent.

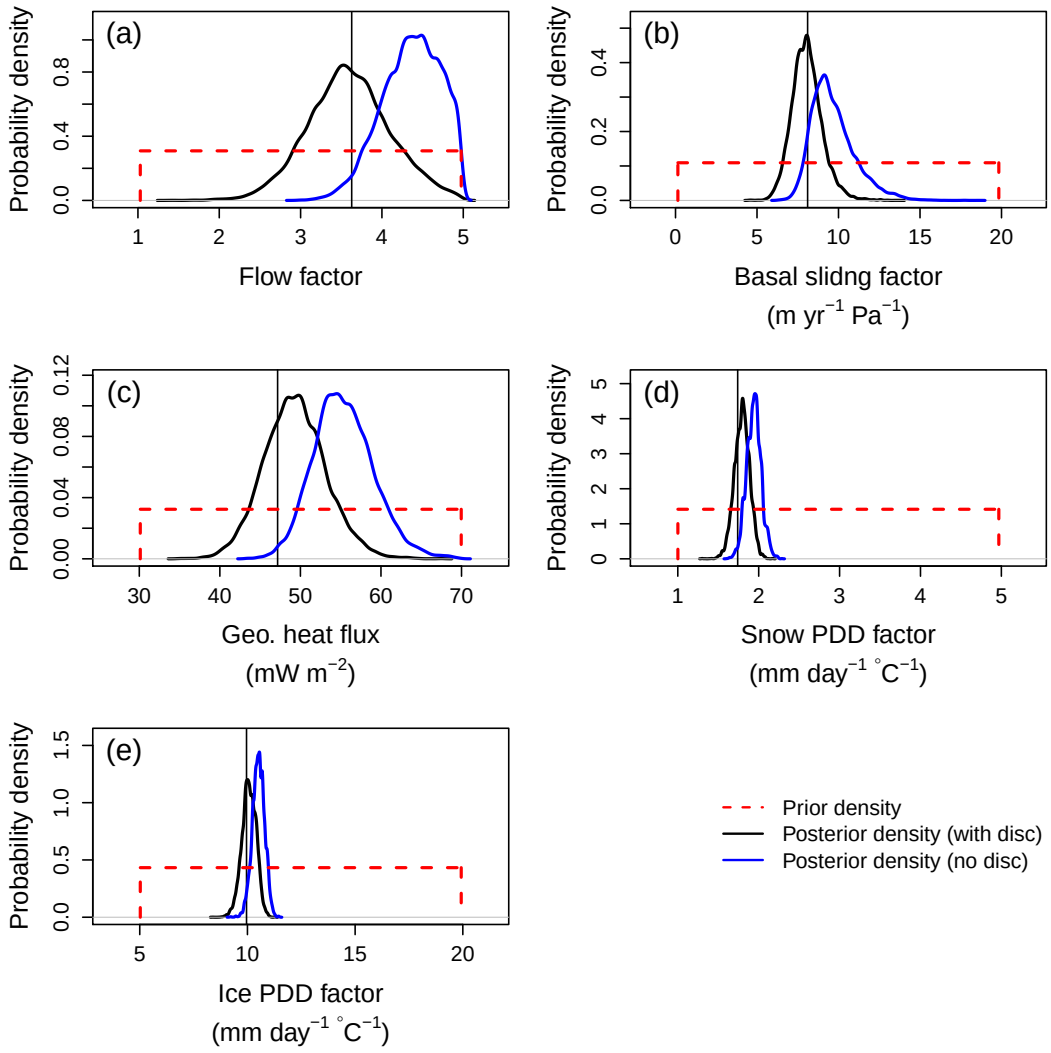

FIG. S2. Comparison between calibration results with and without the discrepancy term $\mathbf{K}_d\boldsymbol{\nu}$ in the calibration model in (S1). In each panel, we tried to learn each of the parameters while fixing the other parameters at their assumed-true values. The prior densities are assumed to be uniform over a broad range (dashed red lines). While the posterior densities computed by including the discrepancy term in the model (solid black curves) pick up the true parameter values without notable biases, the posterior densities without the discrepancy term (solid blue curves) cannot recover the true values.

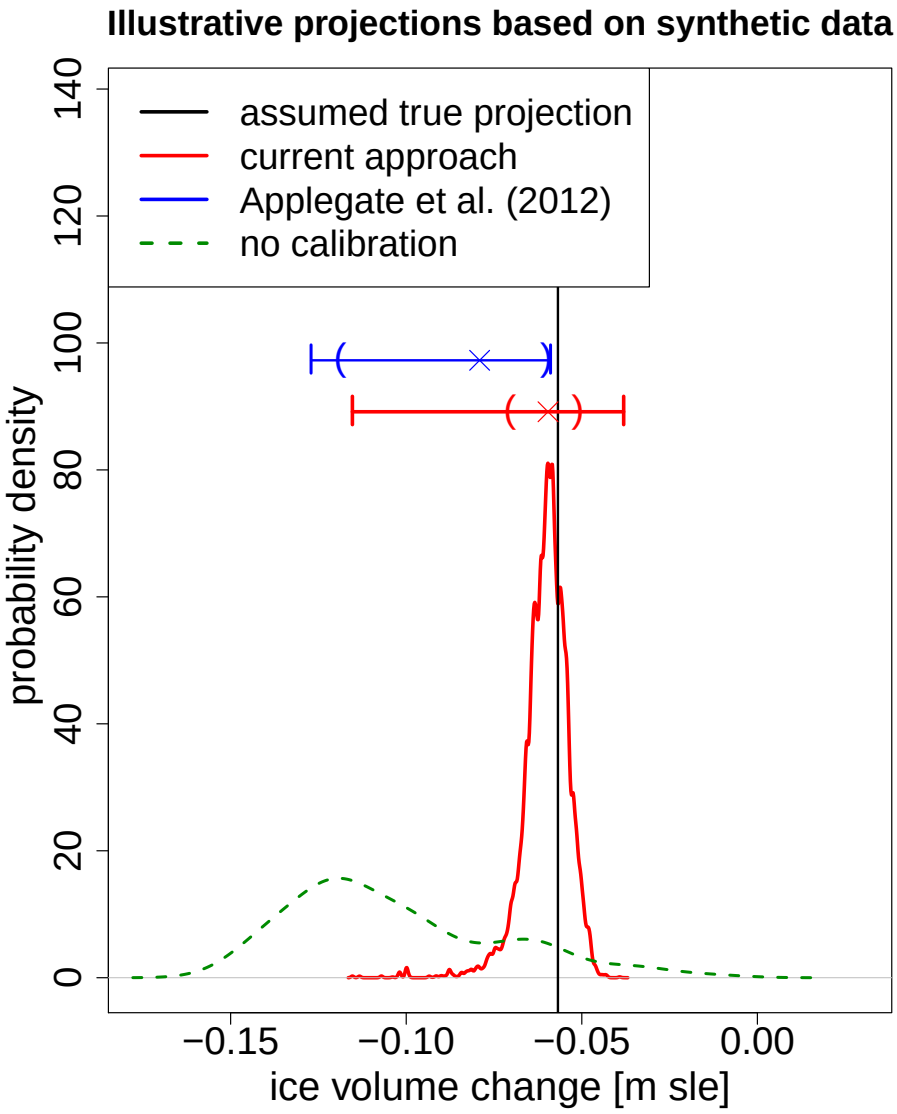

FIG. S3. Illustrative (not "real") ice volume change projections between 2005 and 2100 for model run #23 in Applegate et al. (2012), based on three different methods: i) the prior density of the input parameters (dashed green line); ii) parameter settings that pass the 10% ice volume filter used by Applegate et al. (2012) (solid blue line); and iii) the posterior density computed by our calibration approach (solid red line). The model run has the smallest projected ice volume change from 2005 to 2100 among the model runs that yield modern ice volume within 15% of the observed modern ice volume. The vertical line shows the ice volume change projection for the assumed-true parameter setting. The horizontal lines and the parentheses on them represent the range and the 95% prediction intervals, respectively; the crosses indicate the median projection from each method.

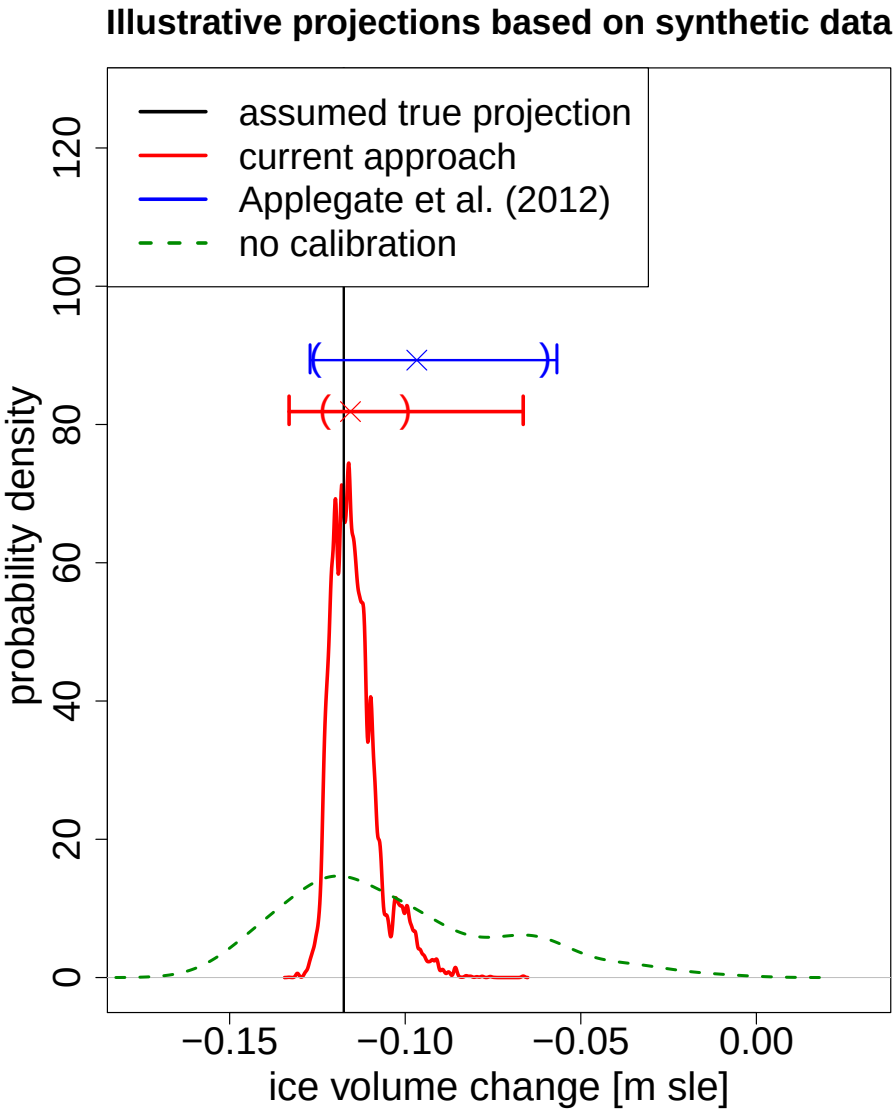

FIG. S4. The same comparison as Figure S3 for the model run #91 in Applegate et al. (2012), which results in the largest projected ice volume change from 2005 to 2100 among the model runs that yields the modern ice volume within 15% of the observed volume.